Chemical Design of Metal Enhanced PEGylated Hydroxyapatite Nanocomposite for Bone Tissue Engineering

Rajeswari Gangadharan[*], Aparnadevi Natarajan and Lakshmi Ravi

Ethiraj College for Women, Chennai – 6000 08, Tamil Nadu, India.

Abstract

Introduction: Current research on reliable skeletal regeneration strategies has focused on the fabrication of biocompatible and biodegradable scaffolds for bone implants. Biocomposites synthesized by blending a polymer with an inorganic phase mimic the composition of natural bone and possesses versatile designing capability, improved biocompatibility and mechanical strength.

Methods: A nano composite of hydroxyapatite (HAp) amalgamated with synthetic biodegradable polymer polyethylene glycol (PEG 6000) and enriched with metallic copper (Cu); HAp/PEG/Cu is successfully synthesized by adopting a three-step chemical process. The physicochemical properties of the synthesized biocomposite are investigated at each stage.

Results: X-ray diffractograms depict the influence of PEG and Cu on the crystallinity of HAp. Fourier transform infrared spectrometry shows the existence of characteristic bands arising due to the molecular interactions between the components of the composite. High resolution scanning electron microscopy studies reveal the rod-shaped morphology, nanoscale particle size distribution and agglomeration states of fine particles. The biocomposite shows synergistic opposition against bacterial growth. Also, non toxicity of the biocomposite is evident from the cytotoxicity study using MTT assay with L6 cell lines.

Conclusion: HAp/PEG/Cu nanobiocomposite could be a promising biomaterial with enhanced mechanical strength and antibacterial effects towards bone tissue regeneration. Also provides suitable environment for cell penetration and adhesion during tissue regrowth.

Keywords: scaffolds, biocomposite, bone implants, hydroxyapatite and biocompatible.

Introduction

The steep rise in occurrences of bone disorders and bone associated chronic diseases especially in aging population, demands need for extensive research on more reliable skeletal regeneration strategies. Recent research focusses on the fabrication of efficacious bone scaffolds

Eur. Chem. Bull. 2023, 12(Issue 8),3349-3365

3349

made up of functional biomaterials which can eliminate the complications associated with the clinical modalities for regeneration of large segmental bone defects. An efficient scaffold for bone should be osteoconductive, integrative and highly porous for nutrient diffusion [1]. The scaffold should facilitate bone ingrowth and its degradation kinetics must be tuned to allow the newly formed tissue to gradually substitute the scaffold. The biomechanical characteristic of the graft material must be analogous to the host bone which allows it to integrate well avoiding undesirable scarring. Synthetic hydroxyapatite (HAp), a calcium phosphate bio ceramic has been widely used as a primary inorganic component of bone scaffolds as its mineral composition is analogous to that of human bone. It has excellent biocompatibility, osteoconductivity and bioactivity [2] but when considered for load bearing applications, it is brittle and has poor mechanical properties [3]. A significant increase in surface area-to-volume ratio and roughness of scaffold is noted on decreasing the material size to the nanoscale, which renders the scaffold with superior physiochemical properties. Nanosized HAp has been reported to display elevated cell adherence and protein assimilation ability for scaffold, thereby improving its biocompatibility [4, 5]. These nanoparticles are also nonimmunogenic and interact with natural tissue without activating inflammation. Moreover, amalgamation of polymeric materials can provide greater control on physiochemical characteristics of scaffolds, promote osteoblast adhesion, migration, differentiation and proliferation. Polyethylene glycol (PEG) is a synthetic polymer with versatile applications in tissue scaffolding due to its biodegradability and segmented block copolymer character [6]. The high hydrophilicity, low toxicity, chain flexibility and its availability in an extensive range of molecular weights makes PEG a suitable choice for scaffolding [7]. PEG also has the ability to act as a surface protector resisting protein adhesion and biological attack It can be readily expelled from the body as non-toxic metabolites [10]. PEG has been reported to impact particle size, crystal phase, degree of aggregation and improve the mechanical compatibility of HAp nanoparticles [11, 12]. Hence scaffolds fabricated for bone implants using biocomposites with two or more components having chemically or physically distinct yet synergistic properties can attain optimal mechanical properties, biocompatibility and controllable degradation rate [13, 14]. Further, the prevention of implant-associated infections caused by microbial adhesions on implant surfaces is of prime importance as it often leads to high morbidity and elevated medical expenses due to surgical revisions [15]. The customary approach to treat infections accompanying orthopedic implants is to administer antibiotics.

Eur. Chem. Bull. 2023, 12(Issue 8),3349-3365

3350

However, the primary concerns with antibiotics adsorbed on the implant surfaces are the growth of resistant microorganisms and rapid wash away by the body fluids making them inefficient in preventing long term post -surgical infections [16]. This difficulty can be overcome by enriching the bone scaffolds with metal ions. Silver, copper and zinc metal ions have been reported to reduce and prevent bacterial adhesion. The possible ways through which metal ions exhibit antimicrobial action are (1) bind with proteins to deactivate them, (2) interact with microbial membranes to cause structural and permeability changes and (3) blend with microbial nucleic acids to prevent microbial replication [17-20].

The present study thus aims at fabricating an organic–inorganic hybrid nano biocomposite enriched with metal ion to mimic the natural bone composition. The composite blends an organic polymer phase for providing toughness and compressive strength, an inorganic phase for bioactivity and a metal ion for imparting antibacterial efficacy. Taking into consideration the properties and functionality of hydroxyapatite nanoparticles (HAp), polyethylene glycol (PEG 6000) and copper (Cu), a synergistic nanocomposite HAp/PEG/Cu has been synthesized and the biological potential of the synthesized composite as smart material in the design of bone tissue scaffolds are examined.

Experimental

(i) Materials

For nano HAp: Precursors used are $(NH_4) H_2 PO_4$ and $Ca(OH)_2$.

For nanocomposite HAp/PEG/Cu: Analytical grade polyethylene glycol of molecular weight 6000g/mol, sodium borohydrate $(NaBH_4)$, $(Ca(NO_3)_2.4H_2O)$, $(CuSO_4.5H_2O)$ are taken as precursors and pellets of sodium hydroxide for pH tuning.

(ii) Synthesis of nanohydroxyapatite

Nano hydroxyapatite (HAP) was prepared adopting sol-gel method with $Ca (OH)_2$ and $(NH_4) H_2 PO_4$ as the Ca and P precursors. For synthesizing stoichiometric nHAp, 100ml of stirred (3h) solution of $Ca(OH)_2$ in ethanol -water mixture (50:50%, v/v) was added dropwise to an equal volume of aqueous solution of $(NH_4) H_2 PO_4$. The proportion of reagents used in synthesis was fixed to ensure a Ca: P molar ratio of 1.67. The resultant mixture was aged for 24 h by stirring while maintaining an alkaline pH of 11. Centrifugation of the obtained sol-gel (15000 rpm for 20min) followed by consecutive sonication with deionized water and ethanol was carried out.

Eur. Chem. Bull. 2023, 12(Issue 8),3349-3365

3351

The residual solid obtained was calcined for 4h at 500° C, ground by mortar and pestle to fine powder.

(iii) Modification of Hydroxyapatite with Polyethylene Glycol and Copper nanometal

The hydroxyapatite was blended with polyethylene glycol (PEG) to form HAp/PEG (HAPP) nanocomposite using sol-gel method. PEG polymer solution prepared by dissolving 4g PEG in 40 ml of deionized water was stirred vigorously for 1 h and kept still for 16h to avoid air bubbles. A 50 ml solution containing 2.36 g of Ca $(NO_3)_2 .4H_2O$ was then added dropwise to the prepared PEG solution under constant stirring for 6 h. It is followed by the addition of 50 ml solution of ammonium dihydrogen phosphate solution prepared by dissolving 0.77 g of $(NH_4) H_2 PO_4$ in deionized water. The mixture was maintained at pH 11 by adding 0.5 M solution of sodium hydroxide NaOH and the obtained HAp/PEG composite gel was centrifuged at 1500 rpm for 20 minutes. The copper nanometal was incorporated in to the prepared HAp/PEG nanocomposite by adding dropwise a solution of 0.0124 g of $CuSO_4.5H_2O$ in 50 ml of deionized water. To this combination, 0.5 M solution of $NaBH_4$ which acts as a reducing agent was finally mixed and stirred for 6 h. The obtained gel was centrifuged at 8500 rpm for 1 h and the resulting solid residue was dried at a temperature of 70° C /8 h to obtain HAp /PEG/ Cu (HAPPC) nanocomposite.

(iv) Physico-chemical characterizations

The crystal structure and the phase of the synthesized nanocomposite was analyzed from X-ray diffractogram recorded from a D8 Advance (Bruker) diffractometer having monochromatic source Cu-K$_{\alpha1}$. The rate of scanning and the step size are 0.5°/min and 0.02° respectively for the measurement over the 2θ angle ranging from 25° to 60°. The surface morphology and distribution of particles were determined using a high-resolution field emission-scanning electron microscopy (FEI-Quanta FEG 200F). Energy dispersive spectroscopic technique has been employed for analyzing elemental composition. Various intermolecular interactions between components in the system were studied from FTIR spectra obtained using the Bruker-Alpha-Platinum single reflection ATR-IR module operating with 2 cm^{-1} resolution in the wave number range of 500-4000 cm^{-1}

Eur. Chem. Bull. 2023, 12(Issue 8),3349-3365

3352

(v) Antibacterial studies

Antibacterial properties of HAPP and HAPPC composites were determined against different bacterial strains using broth dilution method and the minimal inhibitory concentration (MIC) were obtained. A stock solution of 10 mg/ ml test sample was diluted in LB broth and from that different solution concentrations of 62.5mcg, 12.5 mcg, 250mcg and 500 mcg were taken for investigation. Negative control (NC) is the untreated LB broth. A single colony of organism taken from LB streak plate are dissolved and incubated overnight in 3 ml LB broth to get inoculum. Bacterial solution is diluted to obtain 0.1 OD_{600} suspensions which was further incubated with a speed of 220 rpm for 2 h till mid-log phase at 37 °C. 1 ml of this bacterial solution is centrifuged and washed with 1 ml PBS. The obtained bacterial pellet is further diluted (20 µl in 180 µl LB broth) to get the final bacterial concentration of 1 x 10^7 CFU/ml with LB broth (1 OD_{600} ~10^9 CFU/ml) by checking the optical density (OD_{600}) with a spectrophotometer. The bacterial cultures were evenly inoculated to the test sample tubes having varied concentrations [21].

(vi) Cytotoxicity studies

The in-vitro cytotoxicity of HAPP and HAPPC nanocomposites were examined using MTT assay. The viability of the cells treated with the test sample was evaluated through direct observation of these cells with inverted phase contrast tissue culture microscope and quantified by MTT assay method. The test samples were prepared in 10mg/ml DMEM media, filtered and then sterilized. Further these samples were diluted in DMEM media and seeded to the cultured wells at concentrations 6.25µg, 12.5 µg, 25 µg, 50 µg and 100 µg respectively. The control is the untreated wells. In order to minimize errors, experiments was done in triplicate and average values were taken [22]. The test sample plates were incubated for 1 day after treatment. At regular intervals, control and the treated wells were observed up to 24 h in the microscope and photographed. After aspirating and discarding the media, 100 µl of MTT solution in DMEM media was seeded to the wells. Further for the development of formazan crystals, the plates were incubated for 2 - 4 hours. The absorbance at 570 nm after removal of supernatant was measured with micro plate reader. Two wells without cells served as blank.

Eur. Chem. Bull. 2023, 12(Issue 8),3349-3365

3353

The percentage cell viability is evaluated as follows:

$$Percentage\ cell\ viability = \frac{Average\ absorbance\ of\ treated}{Average\ absorbance\ of\ control} \times 100$$
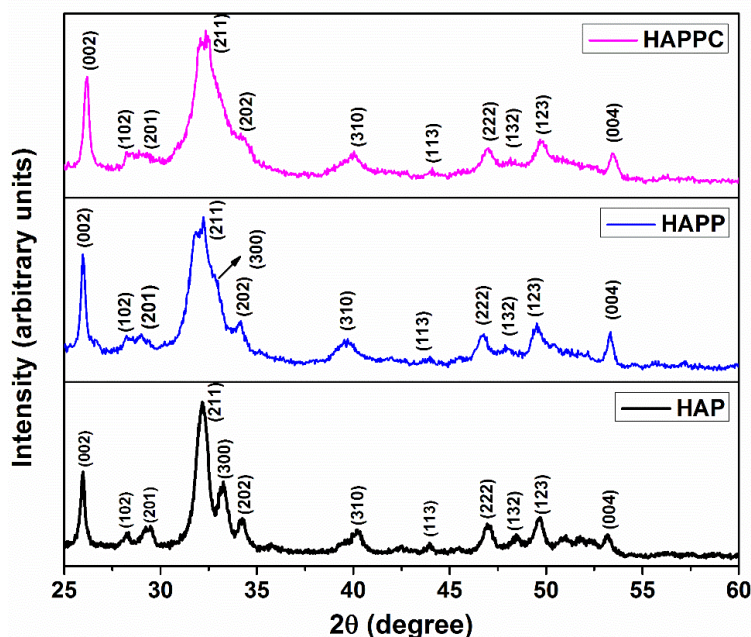
(vii) Swelling Studies

The test samples were soaked in PBS solution for 1 day at 7.4 pH and maintained at 37° C to ensure good adsorption. The wet weight (W_w) of the blotted test samples were recorded [23]. The swelling ratio was determined as follows:

$$Swelling\ ratio = \frac{W_w - W_o}{W_o}$$

W_o being the dry weights of the test material.

Results and Discussions

(i) Structural study

Figure 1: XRD patterns of HAP nanoparticles, HAPP and HAPPC nanocomposites.

The X-ray diffractograms shown in figure 1 track the consistent phase evolution of hydroxyapatite nanoparticles (HAP) into HAp/ PEG (HAPP) and HAp/PEG/Cu (HAPPC) nano composites. The characteristic peaks in the respective diffractogram match well with ICDD data (No. 09–0432). The reflections at 26.12°, 32.11°, 34.28°, 39.68°, 46.86°, 49.71°, 53.34° are consistent with the lattice planes (0 0 2), (1 0 2), (2 1 0), (2 1 1), (3 0 0), (2 0 2), (3 1 0), respectively. This confirms the formation of an apatite phase in HAP, HAPP and HAPPC,

Eur. Chem. Bull. 2023, 12(Issue 8),3349-3365

3354

adopting a single phase hexagonal HAp structure with *P6₃/ₘ* space group. This proves that there is no destabilization or dissolution of hydroxyapatite phase during the inclusion of PEG and copper. The presence of PEG and copper can be inferred from the broadening of peaks in HAPP and HAPPC. Specifically, in the 2θ range 30° to 35° of HAP three distinct peaks indexed (2 0 2), (2 1 1) and (3 0 0) are found whereas in pattern corresponding to HAPP (3 0 0) reflection merges with the pronounced (2 1 1) peak and in HAPPC no traces of (3 0 0) reflection is found and (2 0 2) reflection begin to merge with (2 1 1) peak. Thus, an interaction between the organic and the inorganic components of the composite are evident. Also, the merging of the peaks and the disappearance of the hollow between (2 1 1) and (3 0 0) reflections, indicate lowering of crystallinity and reduced crystallite size as compared to the stoichiometric HAp. It is obvious that the level of crystallinity decreases proportionally with the organic contents of the composite. The reduced crystallinity attributed to the addition of PEG signifies a similarity to the poorly crystallized apatite phases normally found in natural bones [24, 25]. Advantageously, the biomaterial with low crystalline nature will be metabolically more active and soluble in physiological environment in comparison with the well-developed crystalline phase [26]. The mean crystallite sizes obtained from Debye Scherrer equation are shown in Table 1. The FWHM of sharp and distinct diffraction peak at 25.9° assigned to the (0 0 2) reflection was used to estimate the crystallite size. It is found that the crystallite size lies in the nanometer domain and decreases with the incorporation of PEG and copper in HAP. The percentage of crystallinity (X_C) present in the taken volume of sample was evaluated from the relationship [27]

$$B_{002} \sqrt[3]{X_C} = K$$

where constant K is 0.24 for Hap and B_{002} is FWHM (˚) of reflection (002). The calculated percentage of X_C values are found to concur within 10% in majority of practical cases.

Table 1: Average crystallite size distribution and percentage of crystallinity of HAP, HAPP and HAPPC Samples.

Sample	Plane	θ (degree)	FWHM (β) (radian)	Crystallite size (nm)	Crystallinity (%)
HAP	002	13.5642	0.021	7.4333	2.014
HAPP	002	13.4641	0.019	6.7190	1.492
HAPPC	002	13.3107	0.023	6.1310	1.135

Eur. Chem. Bull. 2023, 12(Issue 8),3349-3365

3355

(ii) Morphological study

The surface images of HAP, HAPP and HAPPC were recorded using scanning electron microscopy and are shown in figure 2. The micrograph of HAP reveals homogenous agglomerated rod like structures having particle size of 82.75 nm whereas the image of HAPP shows well-defined and dispersed 68.22 nm sized nano rods. The improved particle behavior with reduction in size, homogeneous distribution and lower agglomeration compared to HAP can be attributed to the functionalization of HAp with PEG. During the synthesis process, PEG molecules surround the metal cation of HAp to form small well-dispersed particles thus lowering the aggregation. More dispersed and less aggregated particles of functionalized HAp are found to be more suitable for use in biomedical applications. Also, the high affinity of HAp towards PEG polymer is evident from the micrograph, as the interface between the components of the composite are indistinguishable in the adopted microscopy scale range. The incorporation of copper metal ion into the composite HAp/PEG is found to have an effect on the grain size. The micrograph of HAPPC shows agglomerated rod like structures with the average grain size being further reduced to about 66.64 nm compared to HAP and HAPP. Moreover, the particle size obtained for the prepared HAp/PEG/Cu nanocomposite is found to be equivalent to that of natural bone apatite thus suggesting its suitability for bone regeneration applications.

Eur. Chem. Bull. 2023, 12(Issue 8),3349-3365

3356
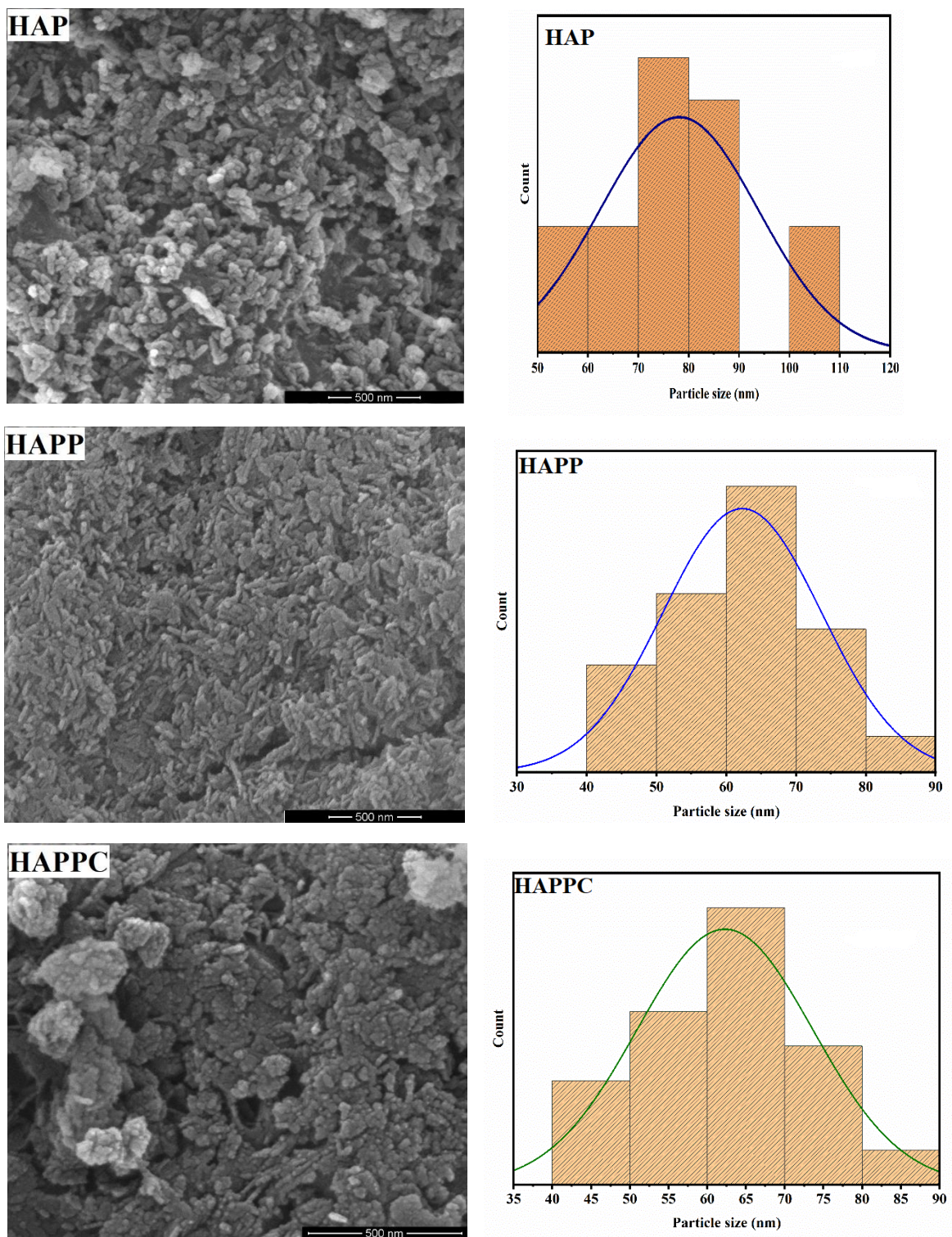
Figure 2: SEM micrographs of HAP, HAPP and HAPPC revealing the rod-shaped nanoparticles and the corresponding histogram showing the average particle size

Eur. Chem. Bull. 2023, 12(Issue 8),3349-3365

3357

(iii) Elemental analysis

The composition of the elements present in the synthesized nanocomposites was investigated using energy dispersive spectroscopy. The EDS images of HAPP and HAPPC samples are shown in figure 3. The spectrum confirms the existence of mineral composition calcium, phosphorous and oxygen in HAP. The appearance of the organic content, carbon in HAPP indicates the presence of PEG. Furthermore, the ratio Ca: P of the nanocomposite is approximately 1.67 and is analogous with the natural bone. The existence of Cu peak in the EDS image of HAPPC validates the incorporation of copper nanoparticles. It is also established that there is absence of other impurities including carbonaceous species in the nanocomposites.
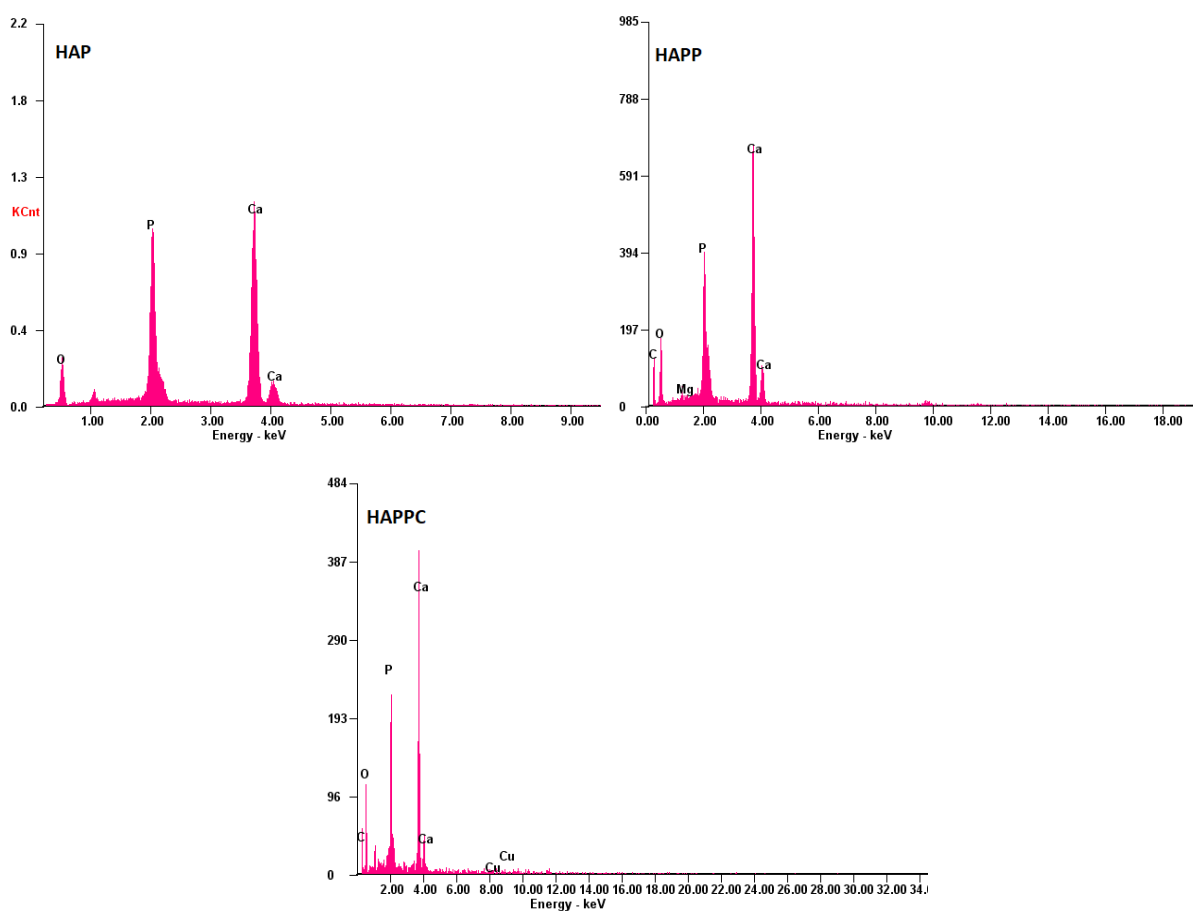

Figure 3: EDS spectra of HAP, HAPP and HAPPC confirming the elemental compositions.

Eur. Chem. Bull. 2023, 12(Issue 8),3349-3365

3358

(iv) FTIR analysis

The intermolecular interactions between the components of the nanocomposite system were illustrated from the FTIR study of HAP nanoparticles, HAPP and HAPPC nanocomposites in the region 4000-500 cm^{-1}. The spectra depicted in figure 4 exhibits functional groups and characteristics bands corresponding to the different molecular interactions of HAP nanoparticles, HAPP and HAPPC nanocomposites. The band observed in the range 560 – 563 cm^{-1} and at 1025 cm^{-1} in all three samples can be attributed to the symmetric P-O band (first) caused by bending modes of the regular tetrahedral PO_4^{3-} groups. The well-defined sharp peak at 602.37 cm^{-1} indicates the bending vibration of the phosphate symmetric P-O band (fourth) of PO_4^{3-}. The stretching mode corresponding to phosphate band (third) is identified at 962.20 cm^{-1}. The bands at 1416.34 cm^{-1} and between 871.72 - 873 cm^{-1} corresponds to the carbonate adsorption. The presence of carbonate ions is due to the adsorption of CO_2 by apatite in the nanocomposite at ambient temperature. The structural apatite –OH band at 3407.8 cm^{-1} is noted in HAPP. The new band observed at 2940 cm^{-1} in HAPP represents the C-H stretching of PEG. This confirms the chemical bond interactions between HAp and PEG. The characteristic peaks in the range 1644 - 1648 cm^{-1} are ascribed to H_2O group. A broad area covered under the band at 3470 cm^{-1} is caused by the hydroxyl group in HAPPC which arises due to the copper ions interaction with the hydroxyl groups of hydroxyapatite. The wave numbers corresponding to the band and their attributions are listed in table 2.

Table 2: FTIR characteristics peaks for HAP, HAPP and HAPPC samples.

Band positions (cm^{-1})			Attributions
HAP	**HAPP**	**HAPPC**	**-**
560 - 563	560 - 563	560 - 563	OPO bending
602.37	602.37	602.37	OPO bending
871 - 873	871 - 873	871 - 873	CO stretching
962.20	962.20	962.20	PO stretching
1025.14	1025.14	1025.14	PO stretching
1416	1416	1416	CO bending
1644 -1648	1644 -1648	1644 -1648	H_2O group
	2940	2940	CH stretching
	3470.8	3470.8	OH group

Eur. Chem. Bull. 2023, 12(Issue 8),3349-3365

3359
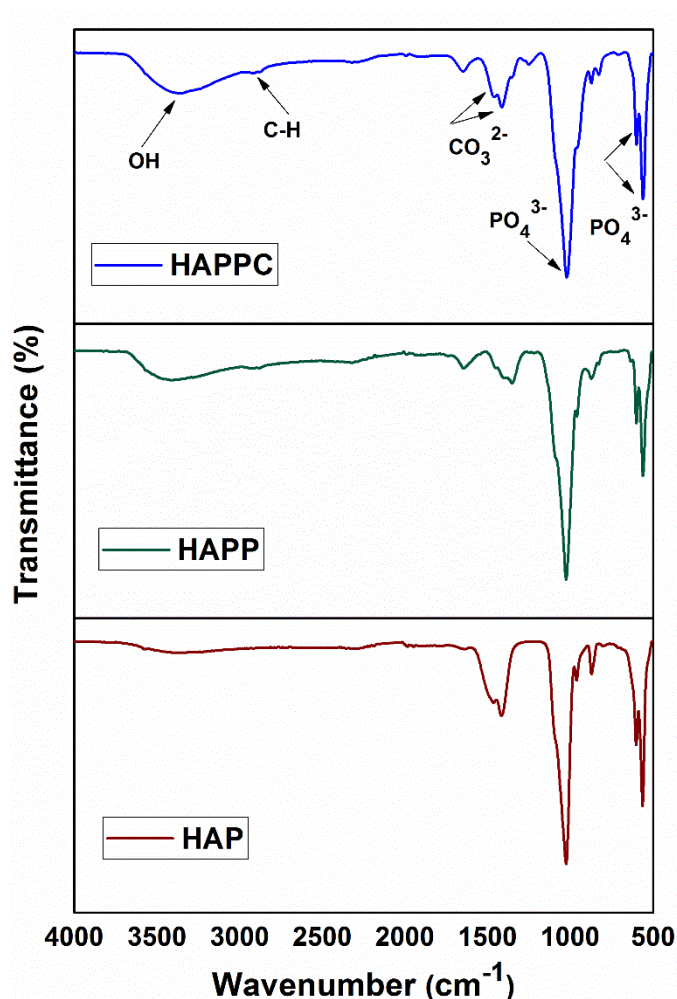
Figure 4: FTIR spectra depicting the characteristic bands of HAP, HAPP and HAPPC.

(v) Invitro studies

### a) *Antibacterial activity*

Bactericidal action of a compound depends on its chemical structure, the type of bacteria and the solvent used for the test. The antibacterial efficacy of HAPP and HAPPC composites was observed using bacterial variants, Staphylococcus aureus and Escherichia coli. Table 3 lists the minimal inhibitory concentration (MIC) for HAPP and HAPPC samples. Under defined test settings, the lowest amount of the assayed sample, inhibiting the bacterial growth is called minimal inhibitory concentration. MIC evaluates the antimicrobial action of new agents and the susceptibility of bacterial strains to that agent. In broth dilution method definite number of bacteria are injected into a liquid growth medium containing geometrically cumulative concentrations of antimicrobial agent. The occurrence of turbidity or a residue in the medium

Eur. Chem. Bull. 2023, 12(Issue 8),3349-3365

3360

after incubation, confirms the growth of an organism. From table 3, it is inferred that with an increase in the concentration of HAPP and HAPPC nanocomposites, growth of bacteria was proficiently reduced. This could be due to the varied collaborate activity of the components present in the composites such as production of reactive oxygen species, inactivation of vital enzymes of bacteria and destruction of bacterial wall. The growth dynamics of selected bacterial strains relative to the control was effectively influenced by the infusion of Cu in nanocomposite and this can be attributed to the denaturizing of proteins by the controlled release of Cu ions from HAPPC composite. The broth with bacterial strain showed no solution turbidity at 500 mcg concentration which can be considered as the endpoint i.e., the lowest concentration of the test sample with no visible growth of bacteria. At this concentration the nanocomposite acts as a potent bactericide leading to a rapid decrease of bacterial growth. The observed significant bactericidal action against both the bacterial variants evidences that HAPPC nanocomposite can be a potent antibacterial source for bone implants.

Table 3: Determination of Minimum Inhibitory Concentration of HAPP and HAPPC for E. coli and S. Aureus bacterial strains.

Organism	Concentration (mcg)	HAPP		HAPPC	
		Absorbance	**Inference**	**Absorbance**	**Inference**
E. Coli	62.5	0.813	Turbid	0.885	Turbid
	125	0.748	Turbid	0.854	Turbid
	250	0.605	Turbid	0.753	Turbid
	500	**0.577**	**No turbidity**	**0.723**	**No turbidity**
	Control	0.781		0.781	
S. Aureus	62.5	0.681	Turbid	0.832	Turbid
	125	0.667	Turbid	0.763	Turbid
	250	0.648	Turbid	0.678	Turbid
	500	**0.544**	**No turbidity**	**0.607**	**No turbidity**
	Control	0.723		0.723	

Eur. Chem. Bull. 2023, 12(Issue 8),3349-3365

3361

b) *Cytotoxicity studies*
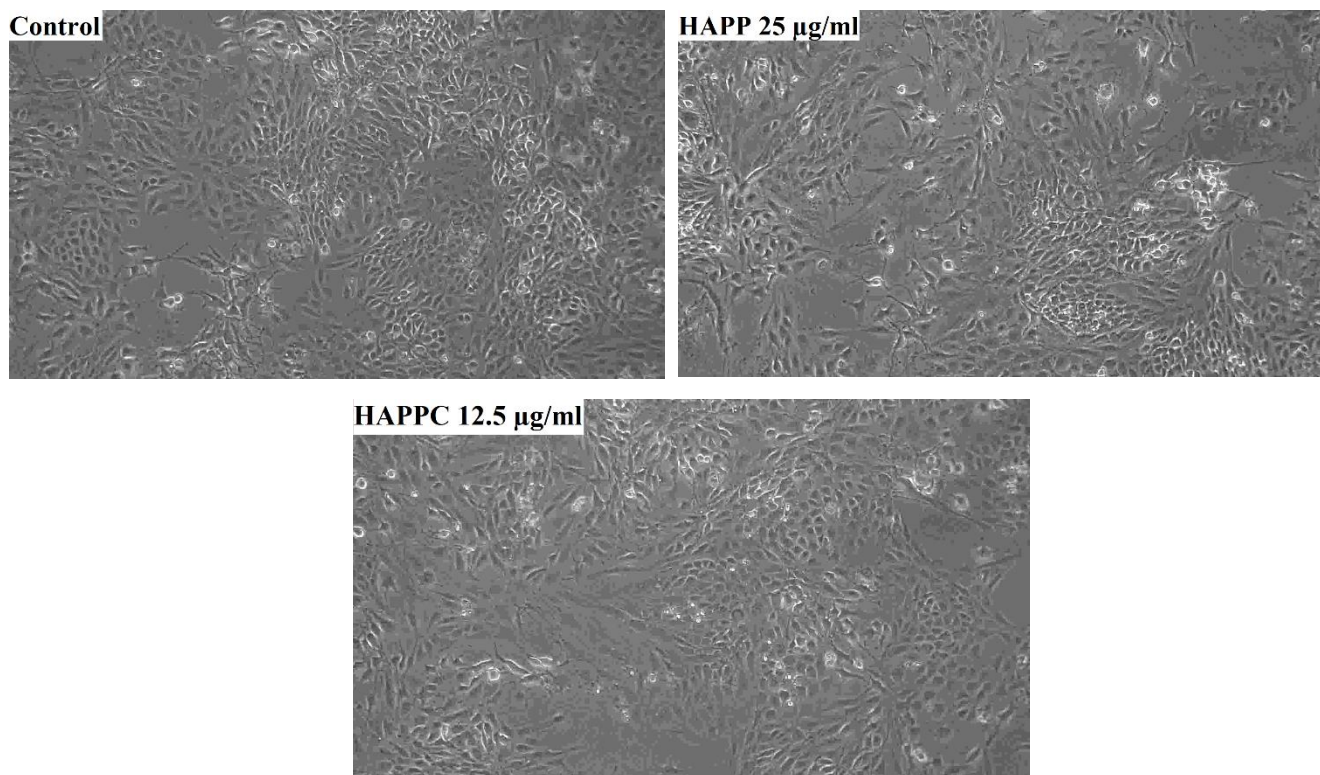
Figure 5: Maximum cell viability shown by HAPP and HAPPC at different concentrations relative to the control.

The cytotoxicity of the synthesized HAPP and HAPPC biocomposites were determined based on the MTT assay test. Figure 5 shows the cell viability after incubation with different concentrations of HAPP and HAPPC biocomposites. The evaluation of cell viability through direct observation shows no visible changes on cell surface, cell volume and no vacuolization in the cytoplasm. The nonappearance of morphological changes indicated the non-cytotoxicity of HAPP and HAPPC biocomposites. Further, quantitative calorimetric test based on the performance of viable cells to reduce tetrazolium yellow salt of the assay into purple formazan insoluble crystals was performed to analyze the cytotoxicity of HAPP and HAPPC biocomposites. Cell viability with different concentrations of HAPP and HAPPC biocomposites are listed in table 4. Subsequent to 24 h incubation over 90% cell viability was found with different concentrations between 6-100 µg/ml of HAPP and HAPPC biocomposites. Percentage of viability was found to increase with concentration up to 25 µg/ml and 12.5 µg/ml for HAPP

Eur. Chem. Bull. 2023, 12(Issue 8),3349-3365

3362

and HAPPC respectively. Above these concentrations viability decreases for both HAPP and HAPPC composites, however cellular metabolic activity did not change much in comparison with the control cells, signifying the non-toxicity of the biocomposites to the mammalian cells. Hence HAPP and HAPPC nano biocomposites can be considered as biocompatible.

Table 4: Cell viability with different concentrations of HAPP and HAPPC biocomposites examined using MTT assay.

	Concentration (µg/ml)	Triplicate 1	Triplicate 2	Triplicate 3	Average	Percentage viability
HAPP (HAp/PEG)	Control	0.975	0.981	0.986	0.980	
	6.25	0.907	0.912	0.921	0.913	93.16
	12.5	0.924	0.929	0.933	0.928	94.69
	25	0.937	0.953	0.961	0.950	96.93
	50	0.886	0.873	0.865	0.874	91.00
	100	0.860	0.875	0.892	0.875	89.28
HAPPC (HAp/PEG /Cu)	Control	0.980	0.986	0.988	0.984	
	6.25	0.966	0.953	0.941	0.953	96.84
	12.5	0.972	0.983	0.987	0.980	99.59
	25	0.950	0.953	0.967	0.956	97.15
	50	0.946	0.930	0.926	0.934	94.91
	100	0.889	0.882	0.871	0.880	89.43

c) Swelling studies

The effect of PEG and Cu on the swelling ratio of the HAPP and HAPPC biocomposites were studied using Phosphate buffered saline (PBS). Factors such as porosity, surface area between the pores, crosslinking, content of filler and physiochemical nature of materials of composite decides the adsorption of PBS. The swelling ratio of HAPP and HAPPC in PBS solution are given in table 5. At 37° C after an interval of 24 h, the nano biocomposites retained PBS and weighed more than the original weight. The results showed that HAPP samples displayed lower swelling ratio as compared to the HAPPC matrix. The incorporation of copper led to an increase in swelling by 3%.

Table 5: Swelling ratio of HAPP and HAPPC biocomposites in PBS solution

Sample	W_o	W_w	Swelling ratio, $\dfrac{W_w - W_o}{W_o}$
HAPP	10.00	10.07	0.007
HAPPC	10.00	10.10	0.01

Eur. Chem. Bull. 2023, 12(Issue 8),3349-3365

3363

(vi) Conclusion

Hydroxyapatite nanoparticles, HAp/PEG (6000 g/mol) and HAp/PEG/Cu nanocomposites were synthesized through a three-step wet chemical sol gel method. The phase at every step were confirmed from X-ray diffractograms. The amalgamation of PEG and Cu do not destabilize the hydroxyapatite phase however the average crystallite size decreases correspondingly. The SEM analysis revealed the rod-shaped morphology of the nanoparticles in HAP, HAPP and HAPPC and reduced particle size of the composites relative to HAP. Functionalization with PEG lowered the agglomeration of the particles in HAPP whereas incorporation of copper instigated agglomeration. Further, EDS spectrum revealed the presence of elemental compositions. FTIR studies established the presence of functional groups and intermolecular interaction between the hydroxyapatite and polyethylene glycol molecules. The nanocomposite was found to be a potent candidate of antibacterial biocide effective for both the bacterial strains, showing significant reduction in bacterial densities at a concentration of 500 mcg. Also, the non-toxic nature of nanocomposites to the mammalian L6 cell lines was determined from the cytotoxicity studies. Hence biocomposite HAp/PEG/Cu could be a viable antibacterial and biocompatible material for bone tissue regeneration providing good mechanical strength and favorable environment for cell penetration and adhesion during tissue regrowth. Further, parameters such as molecular weight of PEG, concentration of PEG & Copper, stirring time and pH can be optimized for improved physiochemical and bioactivity of HAp/PEG/Cu biocomposite.

Eur. Chem. Bull. 2023, 12(Issue 8),3349-3365

3364

References

1.   T. M. Freyman, I. V. Yannas and L. J. Gibson, *Progress in Materials Science* **46** 3, 273-282 (2001).
2.   M. O. Li, X. Xiao, R. Liu, C. Chen and L. Huang, *Journal of Materials Science: Materials in Medicine* **19** 2, 797-803 (2008).
3.   Y. Ding, J. Liu, H. Wang, G. Shen and R. Yu, *Biomaterials* **28** 12, 2147-2154 (2007).
4.   H. W. Kim, J. C. Knowles and H. E. Kim, *Journal of Biomedical Materials Research Part A: An Official Journal of The Society for Biomaterials, The Japanese Society for Biomaterials, and The Australian Society for Biomaterials and the Korean Society for Biomaterials* **72** 2, 136-145 (2005).
5.   M. Peter, N. Ganesh, N. Selvamurugan, S. Nair, T. Furuike, H. Tamura and R. Jayakumar, *Carbohydrate polymers* **80** 3, 687-694 (2010).
6.   F. E. Wiria, C. K. Chua, K. F. Leong, Z. Y. Quah, M. Chandrasekaran and M. W. Lee, *Journal of Materials Science: Materials in Medicine* **19** 3, 989-996 (2008).
7.   A. Bhowmick, N. Pramanik, P. J. Manna, T. Mitra, T. K. R. Selvaraj, A. Gnanamani, M. Das and P. P. Kundu, *RSC advances* **5** 120, 99385-99393 (2015).
8.   J. M. Harris, *Poly (ethylene glycol) chemistry: biotechnical and biomedical applications*. (Springer Science & Business Media, 1992).
9.   J. H. Lee, H. B. Lee and J. D. Andrade, *Progress in polymer science* **20** 6, 1043-1079 (1995).
10. S. D. Jazayeri, A. Ideris, Z. Zakaria, K. Shameli, H. Moeini and A. R. Omar, *Journal of controlled release* **161** 1, 116-123 (2012).
11. Y.-H. Tseng, C.-S. Kuo, Y.-Y. Li and C.-P. Huang, *Materials Science and Engineering: C* **29** 3, 819-822 (2009).
12. N. Rameshbabu, T. Sampath Kumar, T. Prabhakar, V. Sastry, K. Murty and K. Prasad Rao, *Journal of Biomedical Materials Research Part A* **80** 3, 581-591 (2007).
13. N. Pramanik, P. Bhargava, S. Alam and P. Pramanik, *Polymer composites* **27** 6, 633-641 (2006).
14. M. Jayabalan, K. Shalumon, M. Mitha, K. Ganesan and M. Epple, *Acta Biomaterialia* **6** 3, 763-775 (2010).
15. W. Zimmerli, A. Trampuz and P. Ochsner, *The New England journal of medicine* **351**, 1645-1654 (2004).
16. V. Stanić, D. Janaćković, S. Dimitrijević, S. B. Tanasković, M. Mitrić, M. S. Pavlović, A. Krstić, D. Jovanović and S. Raičević, *Applied Surface Science* **257** 9, 4510-4518 (2011).
17. G. Borkow and J. Gabbay, *Current medicinal chemistry* **12** 18, 2163-2175 (2005).
18. B. Sugarman, *Reviews of infectious diseases* **5** 1, 137-147 (1983).
19. S. ATMACA, G. Kadri and R. Cicek, *Turkish Journal of Medical Sciences* **28** 6, 595-598 (1998).
20. T. N. Phan, T. Buckner, J. Sheng, J. Baldeck and R. Marquis, *Oral microbiology and immunology* **19** 1, 31-38 (2004).
21. I. Wiegand, K. Hilpert and R. E. Hancock, *Nature protocols* **3** 2, 163-175 (2008).
22. T. Mosmann, *Journal of immunological methods* **65** 1-2, 55-63 (1983).
23. K. Sahithi, M. Swetha, M. Prabaharan, A. Moorthi, N. Saranya, K. Ramasamy, N. Srinivasan, N. Partridge and N. Selvamurugan, *Journal of biomedical nanotechnology* **6** 4, 333-339 (2010).
24. G. Montel, G. Bonel, J. Heughebaert, J. Trombe and C. Rey, *Journal of Crystal Growth* **53** 1, 74-99 (1981).
25. E. Paschalis, F. Betts, E. DiCarlo, R. Mendelsohn and A. Boskey, *Calcified tissue international* **61** 6, 487-492 (1997).
26. H.-M. Kim, Y. Kim, S.-J. Park, C. Rey, H. Lee, M. J. Glimcher and J. S. Ko, *Biomaterials* **21** 11, 1129-1134 (2000).
27. E. Landi, A. Tampieri, G. Celotti and S. Sprio, *Journal of the European Ceramic Society* **20** 14-15, 2377-2387 (2000).

Eur. Chem. Bull. 2023, 12(Issue 8),3349-3365

3365